AGU100 ADVANCING EARTH AND SPACE SCIENCE

Geochemistry, Geophysics, Geosystems

RESEARCH ARTICLE
10.1029/2018GC007908

Key Points:
- Secondary ion mass spectrometry confirms gametogenic calcite has higher $\delta^{18}O$ values than pregametogenic calcite in *Trilobatus sacculifer*
- Dissolution preferentially removes pregametogenic calcite without altering surface texture of shells
- Dissolution biases whole-shell $\delta^{18}O$ values toward high-$\delta^{18}O$ gametogenic calcite

Supporting Information:
- Supporting Information S1
- Table S1
- Table S2
- Data Set S1
- Data Set S2
- Data Set S3

Correspondence to:
J. B. Wycech,
jody.wycech@colorado.edu

Citation:
Wycech, J. B., Kelly, D. C., Kitajima, K., Kozdon, R., Orland, I. J., & Valley, J. W. (2018). Combined effects of gametogenic calcification and dissolution on $\delta^{18}O$ measurements of the planktic foraminifer *Trilobatus sacculifer*. *Geochemistry, Geophysics, Geosystems*, *19*, 4487–4501. https://doi.org/10.1029/2018GC007908

Received 27 AUG 2018
Accepted 17 OCT 2018
Accepted article online 20 OCT 2018
Published online 14 NOV 2018

Combined Effects of Gametogenic Calcification and Dissolution on $\delta^{18}O$ Measurements of the Planktic Foraminifer *Trilobatus sacculifer*

Jody B. Wycech[1,2], Daniel Clay Kelly[1], Kouki Kitajima[1], Reinhard Kozdon[3], Ian J. Orland[1], and John W. Valley[1]

[1]Department of Geoscience, University of Wisconsin-Madison, Madison, WI, USA, [2]Now at Cooperative Institute for Research in Environmental Science (CIRES), University of Colorado Boulder, Boulder, CO, USA, [3]Lamont-Doherty Earth Observatory, Columbia University, Palisades, NY, USA

Abstract Oxygen isotope ratios ($\delta^{18}O$) measured from planktic foraminifer shells are commonly used to reconstruct past surface ocean conditions, yet the shells of many planktic foraminifers are an aggregate mixture of multiple carbonate phases with differing $\delta^{18}O$ compositions. Here we demonstrate how secondary ion mass spectrometry can be used to measure intrashell $\delta^{18}O$ heterogeneity by performing in situ analyses on micrometer-scale (3–10 μm) domains within individual shells of the extant, mixed layer species *Trilobatus sacculifer*. Secondary ion mass spectrometry measurements on shells taken from Holocene-aged sediments at three sites in different ocean basins confirm that the $\delta^{18}O$ of gametogenic (GAM) calcite added to shells during the terminal (reproductive) stage of the life cycle is 1.0–1.4‰ higher than that of pregametogenic calcite. Examination of shells in cross section reveals that many have suffered varying degrees of internal dissolution, which further skews whole-shell $\delta^{18}O$ compositions toward higher values by preferentially removing low $\delta^{18}O$ pregametogenic calcite. The results of this study echo the calls of earlier studies cautioning that spatiotemporal changes in the proportion of high $\delta^{18}O$ GAM calcite should be considered when assessing *T. sacculifer* $\delta^{18}O$ records generated via conventional isotope ratio mass spectrometry.

Plain Language Summary Foraminifera are unicellular marine organisms that grow microscopic shells made of the mineral calcite. Foraminifer shells are commonly preserved in deep-sea sediments, and their whole-shell chemistries are analyzed to reconstruct the history of ocean climate change. However, these analyses can be problematic because some foraminifera add multiple calcite phases with differing chemistries during their life cycle. Here we use a novel analytical technique called secondary ion mass spectrometry to measure oxygen isotope ratios on minute spots within individual shells of the planktic foraminifer, *Trilobatus sacculifer*. Our results show that whole *T. sacculifer* shells are a mixture of two geochemically distinct calcite phases—one with low oxygen isotope ratios that formed near the warm sea surface and one with high oxygen isotope ratios that formed as the shells sink into colder water. Hence, addition of secondary calcite in deeper water elevates whole-shell oxygen isotope values and introduces inaccuracies into sea surface reconstructions derived from conventional measurements. Images of the shells in cross section reveal that this inaccuracy in whole-shell measurements is compounded by the preferential dissolution of the internal calcite. Our study illustrates potential issues with whole-shell oxygen isotope measurements and demonstrates how secondary ion mass spectrometry analysis can improve the fidelity of sea surface reconstructions.

1. Introduction

Oxygen isotope ratios ($\delta^{18}O$) measured from the calcite shells of planktic foraminifera are widely used to generate records of past ocean climate change, yet the use of conventional gas source mass spectrometry (GSMS) to reconstruct surface ocean conditions requires analysis of whole planktic foraminifer shells that are geochemically homogenous. Planktic foraminifer species such as *Globigerinoides ruber* have homogenous $\delta^{18}O$ compositions and are therefore considered reliable carriers of the proxy (e.g., Anand et al., 2003; Lea et al., 2000). However, a failing common to *G. ruber* is that its delicate, thin-walled shells are not preserved at dissolution-prone sites bathed by corrosive bottom waters (Berger, 1968, 1970; Thunell & Honjo, 1981).

When faced with such a taphonomic bias, researchers typically use a different mixed layer dwelling species that has a more continuous fossil record owing to its thicker, more dissolution-resistant shell. Of these thick-shelled taxa, the extant species *Trilobatus sacculifer*—formerly *Globigerinoides sacculifer* (see Spezzaferri et al., 2015)—is the preferred substitute for reconstructing past sea surface conditions at tropical and subtropical sites (e.g., Ford et al., 2015; Wara et al., 2005). Use of *T. sacculifer* for paleoceanographic reconstructions is well justified because field and culturing studies have established the ecological affinities of this symbiont-bearing, mixed layer species (Bé, 1960; Bé et al., 1982; Bijma & Hemleben, 1994; Spero & Lea, 1993), and its $\delta^{18}O_{calcite}$ values have been empirically calibrated against temperature (Mulitza et al., 2003).

Unfortunately, this species is not without its shortcomings. Specifically, surface ocean reconstructions based on such dissolution-resistant foraminifera often suffer from inaccuracies caused by the heterogeneous geochemical compositions of their shells (Lohmann, 1995). This problem is exemplified by *T. sacculifer* whose whole shell composition is an aggregate mixture of two carbonate phases—pregametogenic (PREGAM) and gametogenic (GAM) calcites—grown under different environmental and physiological conditions (Bé, 1980). The rapid addition of a GAM crust to the exterior of *T. sacculifer* shells poses a major problem to paleoceanographic reconstructions because it occurs at the end of the life cycle as the shell sinks into deeper, colder waters during reproduction (Bé, 1980). Hence, GAM calcite tends to have higher $\delta^{18}O$ values than the PREGAM calcite within an individual shell of *T. sacculifer* (Duplessy et al., 1981).

Here we demonstrate how the unwanted effects of gametogenesis on the $\delta^{18}O$ composition of *T. sacculifer* shells can be avoided by in situ measurements on micrometer-scale domains in PREGAM calcite using secondary ion mass spectrometry (SIMS). The high precision and spatial resolution (3–10 μm) of this in situ analytical technique permits isolated $\delta^{18}O$ measurement on a specific calcite phase within an individual foraminifer shell (Kozdon et al., 2009; Wycech et al., 2018). Hence, it holds much promise for removing the secondary signals that complicate $\delta^{18}O$-based paleoclimate records generated with conventional GSMS entailing analysis of whole foraminifer shells. In addition, we evaluate how postdepositional carbonate dissolution alters the original proportion of GAM calcite within individual *T. sacculifer* shells and influences the $\delta^{18}O$ compositions of whole *T. sacculifer* shells.

2. Materials and Methods

2.1. Study Sites and Samples

Shells of the mixed layer dwelling species *T. sacculifer* were extracted from core top (Holocene) sediment samples recovered at Ocean Drilling Program Site 806 in the western equatorial Pacific (Shipboard Scientific Party, 1991), Site A2 in the Caribbean, and Site PC9 in the northwestern Atlantic (Table 1 and Figure 1). The sites were selected from multiple ocean basins to assess how shell preservation and $\delta^{18}O$ values are affected by disparate bottom water chemistry. Furthermore, the mixed layer at Sites 806 and A2 is deeper and more seasonally stable than at Site PC9 (Table 1), which allows us to assess how the upper ocean thermal structure controls intrashell $\delta^{18}O$ heterogeneity of *T. sacculifer* shells. *T. sacculifer* lives year-round at such tropical locations as sites 806 and A2, while its abundances vary seasonally throughout the subtropics (Site PC9) where *T. sacculifer* is more common during the summer months (Bé, 1960; Deuser & Ross, 1989).

Each core top sample was disaggregated for approximately 30 min in a pH-buffered solution (pH ≈ 8) made of sodium hexametaphosphate, hydrogen peroxide (30%$_v$), ammonium hydroxide, and distilled water, then rinsed with tap water over a 63-μm sieve. Resulting coarse-fraction (>63 μm) materials were rinsed with distilled water before being oven dried (30 °C) overnight. *T. sacculifer* shells were handpicked from the 355-425 μm sieve size fraction. All core top *T. sacculifer* shells were opaque (frosty) in appearance except for several translucent (glassy) shells from PC9 (Table S1 in the supporting information). In addition, three *T.* sacculifer shells (530–590 μm) collected by a sediment trap (EqPac) deployed at 2,284 m in the central, equatorial Pacific during 7–24 March 1992 (Honjo et al., 1995) were used for in situ $\delta^{18}O$ analyses (Figure 1 and Table 1). The sediment trap specimens were directly extracted from the 3% formalin, sodium borate buffered seawater solution in 2014 prior to analysis in January 2015. These shells were translucent (*glassy*) in appearance, exhibiting pristine internal and external wall textures (Data Sets S1 and S2 and Figure 2) with one PREGAM specimen having intact spines (Figure 2c).

Table 1
Sample Descriptions, Water Depths and Geographic Locations of Study Sites, Age of Core Top Sediments, Observed Mixed Layer Temperatures and $\delta^{18}O_{sw}$ Values, Approximate MLD, Bottom Water Carbonate Ion Conditions, Range of Predicted $\delta^{18}O_{calcite}$ Values for T. sacculifer, and Measured $\delta^{18}O_{calcite}$ Values of T. sacculifer as Determined by Conventional GSMS Analyses (See Section 2.4)

	Site	Core, section, interval (cm)	Water depth (m)	Latitude	Longitude	Sample age (years)	Observed temperature (°C)	Observed $\delta^{18}O_{sw}$ (‰, VSMOW)[g]	Approximate MLD (m)[h]	ΔCO_3^{2-} (μmol/kg)[i]	Predicted $\delta^{18}O_{calcite}$ (‰, VPDB)	GSMS $\delta^{18}O_{calcite}$ (‰, VPDB)[j]
Core top	806	1H-1, 0-2	2,520	0°19.11′N	159°21.68′E	Holocene[a]	27.8–30.0[e]	0.3	120	9	−3.4 to −2.9	−2.0[a]
	A2	0-2	3,070	13°48.13′N	78°57.01′W	Holocene[b]	24.5–28.7[e]	1.2	115	28.1	−2.2 to −1.3	−1.1[b]
	PC9	0-1	2,790	31°55.691′N	75°43.774′W	1,870 ± 40[c]	19.8–29.2[f]	1.0	35	4.1	−2.6 to −0.4	−0.7[k]
Sediment trap	EqPac	NA	2,284	0°04′N	139°45′W	Modern[d]	22–29[e]	0.4	100	−40.3	−3.2 to 0.1	NA

Note. GSMS = gas source mass spectrometry; VSMOW = Vienna standard mean ocean water; MLD = mixed layer depth; VPDB = Vienna Peedee Belemnite. [a]Wara et al. (2005). [b]This study (see section S1). [c]Wycech et al. (2016). [d]Honjo et al. (1995). [e]Mean annual temperatures (0- to 100-m water depth). [f]Mean summer temperatures (0- to 100-m water depth). [g]Sea surface $\delta^{18}O_{sw}$ value measured by Dekens et al. (2002) from sites MW91-9 38 (0°0.35′N, 159°22.0′E), KNR-64 5PG (16°31.3′N, 74°48.4′W), OCE 173-4 G (31°54′N, 64°18′W), and W8402A 14GC (0°57.2′N, 138°57.3′W). Typical error on measurements is ±0.3–0.4‰ (±2 SD; University of California-Santa Cruz Stable Isotope Laboratory). [h]Water depth at the top of the thermocline (Locarnini et al., 2013). [i]Bottom water $\Delta CO_3^{2-} = [CO_3^{2-}]_{in\ situ} - [CO_3^{2-}]_{saturation}$ (Berger et al., 1982) calculated at sites MW91-9 38, KNR-64 5PG, OCE 173-4 G, and W8402A 14GC (Dekens et al., 2002). [j]Values are single measurements of two to three pooled shells. External analytical precision is 0.1‰ (±2 SD). [k]This study.

2.2. Preparation of Specimens for In Situ Analyses

Prior to cross sectioning for SIMS analyses, whole shell images of the specimens were taken using backscattered electron imaging on a Hitachi S-3400 N scanning electron microscope (SEM) in variable pressure mode (Figure 3a and Data Set S1). The *T. sacculifer* shells were subsequently cast within 5 mm of the center of a 25.4-mm diameter epoxy mount along with three grains of the calcite standard UWC-3 ($\delta^{18}O = -17.9$‰ Vienna Peedee Belemnite [VPDB]; Kozdon et al., 2009). The epoxy mount containing the *T. sacculifer* shells and standard grains was ground with a fixed-diamond pad to expose shells in cross section (Kozdon et al., 2011), polished with a diamond suspension to a relief of less than 1 μm (Kita et al., 2009), and gold coated. Four epoxy mounts containing *T. sacculifer* shells were analyzed in this study. Secondary electron (SE) SEM images of each mounted shell were taken in high vacuum mode to assess sample exposure and cross-section geometry prior to in situ analysis (Figure 3b and Data Set S2).

2.3. In Situ $\delta^{18}O$ Measurement by SIMS

The micrometer-scale spatial resolution afforded by SIMS enables $\delta^{18}O$ measurements in different calcite phases (PREGAM and GAM) of an individual foraminifer (Figure 3c). The PREGAM and GAM calcites were distinguished in cross section by (1) position within the shell wall (PREGAM = internal, GAM = external), (2) structural appearance (PREGAM = flaky with many epoxy-filled vacant domains, GAM = dense), and (3) typical separation by a band of epoxy (see section S3). All in situ $\delta^{18}O$ measurements were made within the penultimate chamber of each specimen where the shell wall is composed of both PREGAM and GAM calcites using a CAMECA IMS 1280 ion microprobe at the WiscSIMS Laboratory, Department of Geoscience, University of Wisconsin-Madison. These in situ $\delta^{18}O$ analyses were carried out using a $^{133}Cs^+$ primary ion beam, replicating the instrumental conditions described by Kozdon et al. (2013). Each series of 8–12 in situ measurements of foraminifer calcite $\delta^{18}O$ was bracketed by four to six consecutive analyses of $\delta^{18}O$ in a UWC-3 standard grain mounted in the center of each epoxy mount. The bracketing standard analyses were used to determine instrumental mass fractionation corrections for each set of foraminifer calcite measurements.

Measurements from ~10-μm diameter pits were obtained with a primary ion beam intensity of 1.2 nA. Secondary $^{18}O^-$, $^{16}O^-$, and $^{16}OH^-$ ions were detected from the 10-μm spots using three Faraday cup detectors with a typical $^{16}O^-$ count rate of 2.0×10^9 counts per second. The total analytical time per spot was 3 min including presputtering. The average precision (reproducibility) from the sets of bracketing standard measurements was ±0.3‰ (2 SD, spot to spot). A total of seventy 10-μm SIMS measurements on *T. sacculifer* shells and 59 bracketing measurements on the UWC-3 standard were performed.

A second analytical setup with a primary beam current of 15–18 pA and a spot size of ~3 μm was used to measure small PREGAM domains and thin GAM calcite crust present on some shells. Secondary $^{18}O^-$, $^{16}O^-$, and $^{16}OH^-$ ions were detected simultaneously using two Faraday cups ($^{16}O^-$ and $^{16}OH^-$) and an electron multiplier ($^{18}O^-$) with a typical $^{16}O^-$ count rate of 3.4×10^7 counts per second. The electron multiplier gain was monitored before the third analysis of each group of standard calcite analyses, and, when necessary, the applied high voltage was adjusted to compensate for drift in the electron multiplier gain. The total analytical time per spot was 7 min including presputtering. The average precision (reproducibility) for the 3-μm analyses, as determined from the sets of bracketing standard measurements, was ±0.7‰ (2 SD, spot to spot). A total of sixty-four 3-μm SIMS measurements were performed on *T. sacculifer* shells recovered from the core top and EqPac sediment trap samples in addition to 64 bracketing measurements of the UWC-3 standard.

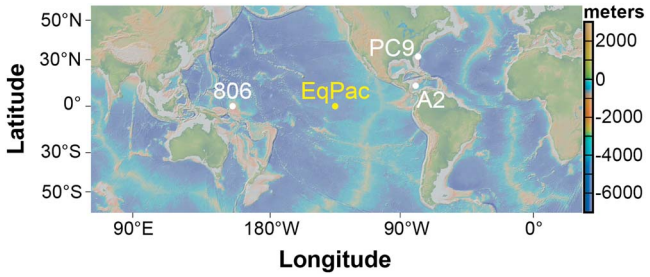

Figure 1. Global bathymetric map showing locations of study sites. White circles mark sites from which the three core top samples were taken, yellow circle marks location of EqPac sediment trap station.

Following SIMS $\delta^{18}O$ measurements, each analysis pit was imaged by SEM using the SE detector in high vacuum mode (Data Set S3). The quality of individual analyses on *T. sacculifer* shells was assessed on the basis of the visual appearance of the pit (Wycech et al., 2018) and the secondary $^{16}O^-$ ion yield (ion count rate/primary beam current) relative to the standard (see section S2 for quality control details). Whenever possible, discrete SIMS $\delta^{18}O$ measurements were performed on the PREGAM (three to four pits per shell) and GAM (one to two pits per shell) calcites of the same shell (Figure 3c). In some cases, paired PREGAM and GAM $\delta^{18}O$ measurements were not obtained from the same shell because the PREGAM calcite did not have suitable domains for in situ analysis and/or the GAM crust was too thin (<3 μm). Such unpaired PREGAM and GAM $\delta^{18}O$ data were still included in the data sets compiled for each site. Average PREGAM and GAM $\delta^{18}O$ values per shell were used to calculate a cumulative average for PREGAM and GAM $\delta^{18}O$ values at each site. All SIMS $\delta^{18}O$ measurements of *T. sacculifer* are reported in Table S1.

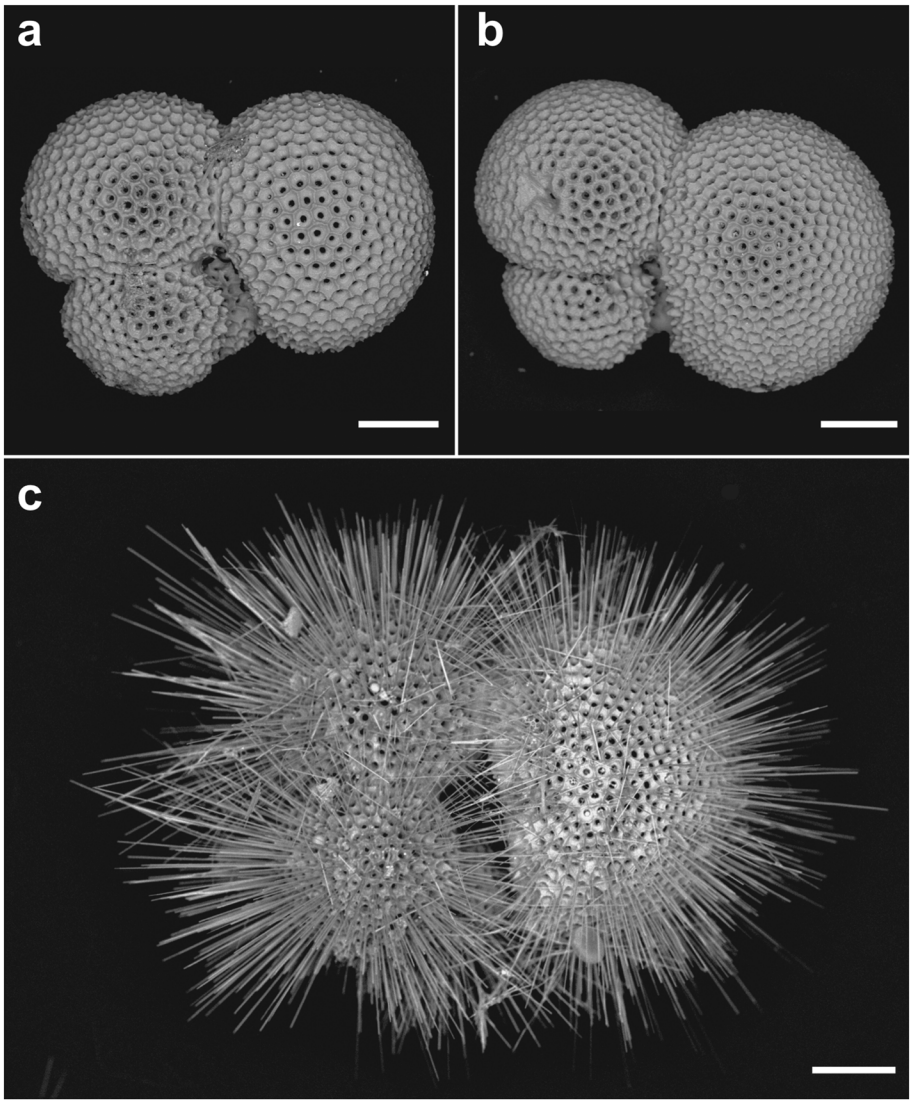

Figure 2. Backscattered electron scanning electron microscope images of three *T. sacculifer* shells from the EqPac sediment trap. (a, b) Postgametogenic (spineless) shells. (c) Pregametogenic shell with intact spines. All scale bars are 100 μm.

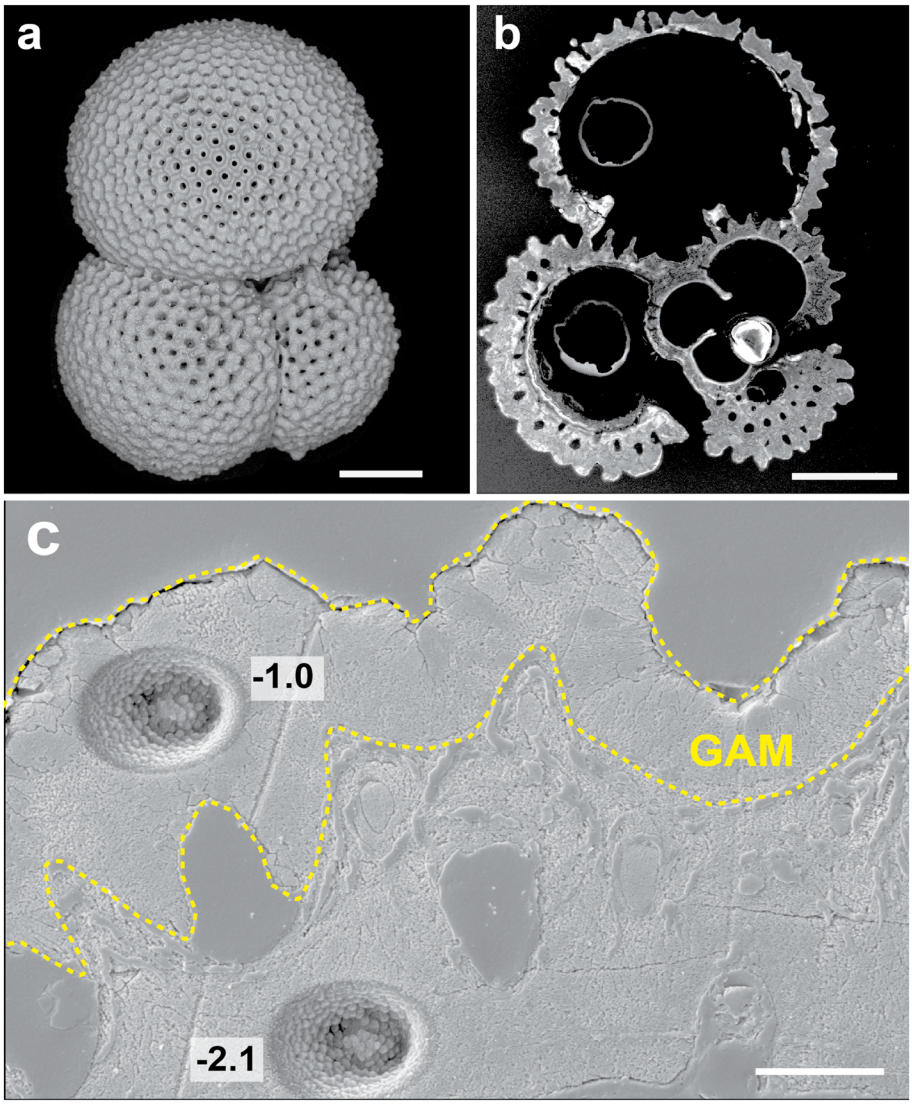

Figure 3. Scanning electron microscope images of a postgametogenic *T. sacculifer* shell from Site A2 core top. (a) Backscattered image showing exterior of shell. (b) Secondary electron scanning electron microscope image showing cross section of shell mounted in epoxy. Scale bars in (a) and (b) are 100 μm. (c) Highly magnified image (scale bar = 10 μm) of penultimate chamber in cross section showing 10-μm secondary ion mass spectrometry analysis pits and corresponding $\delta^{18}O$ values (‰, Vienna Peedee Belemnite). Note: $\delta^{18}O$ values have been adjusted (+0.9‰) using correction determined by Wycech et al. (2018) and gametogenic calcite outlined with yellow dashed line.

2.4. Whole Shell $\delta^{18}O$ Measurement by GSMS

For comparison, complementary $\delta^{18}O$ values were compiled for *T. sacculifer* shells from the core top samples of the three study sites using traditional GSMS. In this study, the GSMS-based $\delta^{18}O$ values of whole *T. sacculifer* shells from sites A2 and PC9 were analyzed at the University of California-Santa Cruz Stable Isotope Laboratory with a ThermoScientific Kiel IV carbonate device interfaced to ThermoScientific MAT-253 dual-inlet gas source isotope ratio mass spectrometer. External analytical precision for $\delta^{18}O$ measurements is 0.06‰ (±2 SD) based on replicate analyses of Carrera Marble on this instrument. Translucent (glassy) *T. sacculifer* shells were measured from site PC9 (250- to 355-μm size fraction; n = 2 shells, pooled). The use of slightly different size fractions for in situ (355–425 μm) and whole shell (250–355 μm) $\delta^{18}O$ measurements at Site PC9 is not considered problematic since the $\delta^{18}O$ of *T. sacculifer* does not exhibit a strong degree of size dependency over the 250–425 μm range (Elderfield et al., 2002; Spero & Lea, 1993). A pooled mixture of glassy and frosty *T. sacculifer* shells (355-425 μm size fraction) were

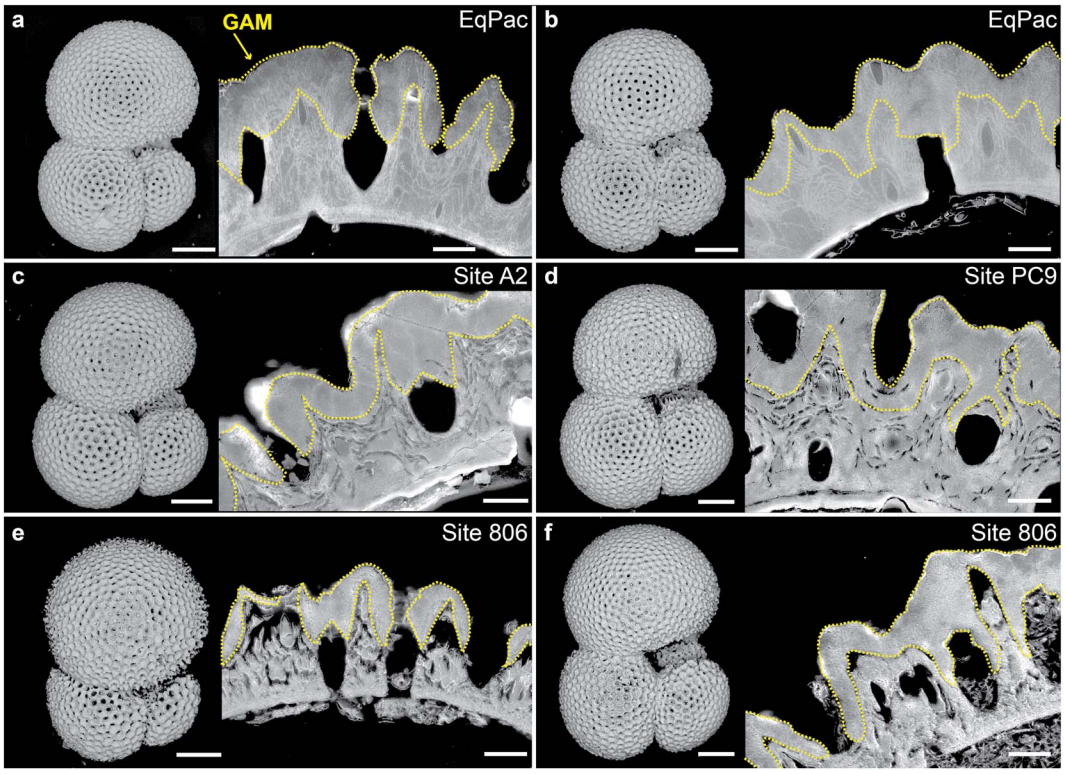

Figure 4. Comparison of external and internal structures of *T. sacculifer* shells from EqPac sediment trap (a, b), and core top samples of sites A2 (c), PC9 (d), and 806 (e, f). Left panels: Backscattered electron scanning electron microscope images showing exteriors of whole shells (scale bars = 100 μm). Right panels: Secondary electron scanning electron microscope images of cross-sectioned penultimate chamber walls of shell in left panel (scale bars = 10 μm). Yellow dashed lines outline dissolution-resistant GAM crust on outermost chamber wall. Note varying degrees of pregametogenic calcite dissolution. GAM = gametogenic.

measured from the core top of Site A2 (n = 3 shells), and previously published GSMS $\delta^{18}O$ values from frosty *T. sacculifer* shells (355-425 μm size fraction) are referenced in this study for the Site 806 core top (Table 1; Wara et al., 2005). The *T. sacculifer* shells from sites A2 and PC9 were not treated chemically or physically (sonicated) prior to GSMS analysis. Complementary GSMS $\delta^{18}O$ analyses were not performed for the EqPac sediment trap sample owing to the limited number of *T. sacculifer* shells recovered.

2.5. Quantitative Constraints on Intrashell Dissolution

Unlike conventional GSMS analysis entailing acid digestion of whole foraminifer shells, in situ $\delta^{18}O$ measurements by SIMS analysis requires that each *T. sacculifer* shell be ground and polished to cross section. The cross-sectioned shells expose the internal structure of each specimen (see section S3), making it possible to measure the relative proportions of PREGAM and GAM calcites. SEM imaging of the cross-sectioned shells revealed that many have suffered internal dissolution that has selectively removed PREGAM calcite without altering their external appearance (Figures 4 and S3). To gauge the effects of this potential bias, image processing software (ImageJ) was used to measure the proportion of GAM calcite present before dissolution and the proportion of PREGAM calcite removed by dissolution. We note that this technique requires that measurements made on the two-dimensional image of the penultimate chamber are representative of the three-dimensional shell. Specifically, the methodology assumes that the proportions of PREGAM and GAM calcites on the imaged chamber reflect the proportions of the whole shell and that PREGAM dissolution occurs uniformly throughout the shell. This technique does not consider the presence of the aperture (i.e., the absence of shell wall) or the lack of GAM calcite on internal (juvenile) chambers. However, the three final chambers of *T. sacculifer* compose the bulk of the

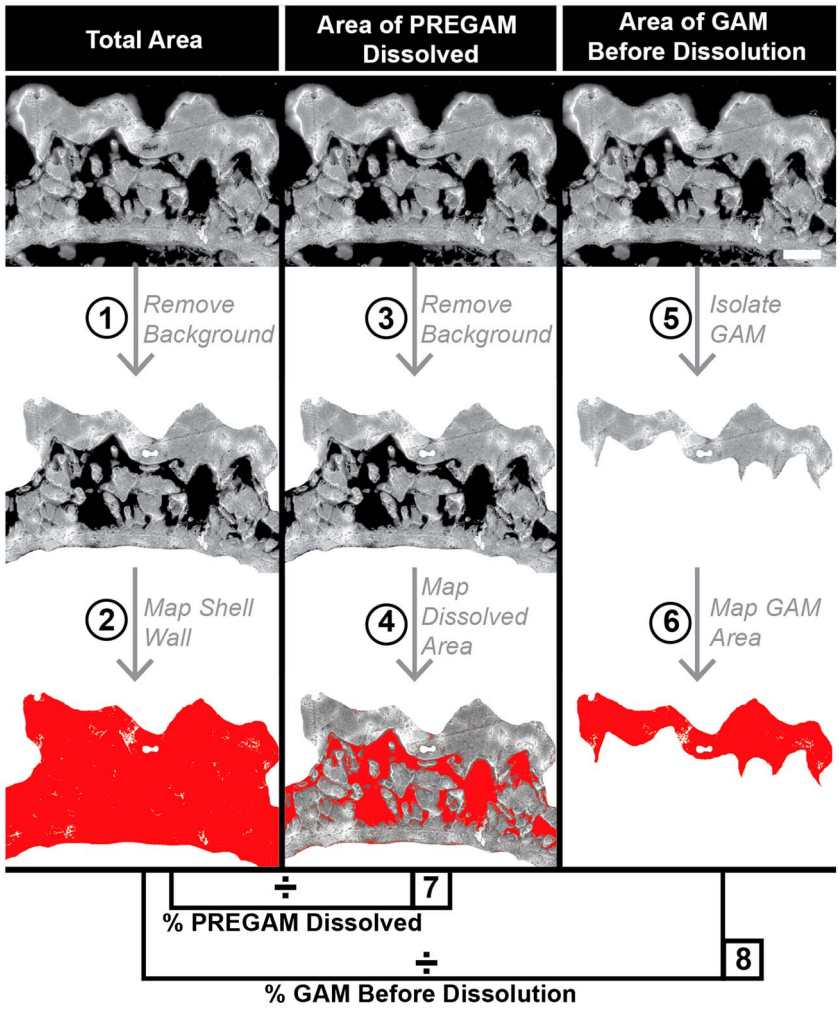

Figure 5. Image processing steps used to quantify the amount of PREGAM calcite removed by dissolution and revise estimates of percentage of GAM calcite in whole shells (scale bars are 10 μm and applicable to all images). All scanning electron microscope images from cross-sectioned penultimate chamber of an individual *T. sacculifer* shell taken from Site 806 core top. Area mapped by ImageJ (red). See section 2.5 for more details. GAM = gametogenic; PREGAM = pregametogenic.

shell, so image processing of the cross-sectioned penultimate chamber walls provides a first-order approximation of the amount of GAM calcite in partially dissolved *T. sacculifer* specimens.

The work flow for image processing is outlined below (see Figure 5):

Steps 1 and 2: Measure total area of penultimate chamber in the frame by removing background using Adobe Photoshop (Step 1) and mapping area of chamber wall (red area) using the threshold tool in ImageJ (Step 2). Select *Analyze Particles* in ImageJ to quantify and output the number of pixels within the mapped area.

Steps 3 and 4: Measure the area of PREGAM calcite dissolved by removing background using Adobe Photoshop (Step 3) and mapping dissolved (black) areas within chamber wall using the threshold tool in ImageJ (black areas ➔ red areas; Step 4). Select *Analyze Particles* in ImageJ to quantify and output the number of pixels within the mapped area.

Steps 5 and 6: Isolate and measure the area of GAM calcite before dissolution by removing imaged areas except GAM crust using Adobe Photoshop (Step 5) then map area of GAM crust (red area) using the threshold tool in ImageJ (Step 6). Select *Analyze Particles* in ImageJ to quantify and output the number of pixels within the mapped area.

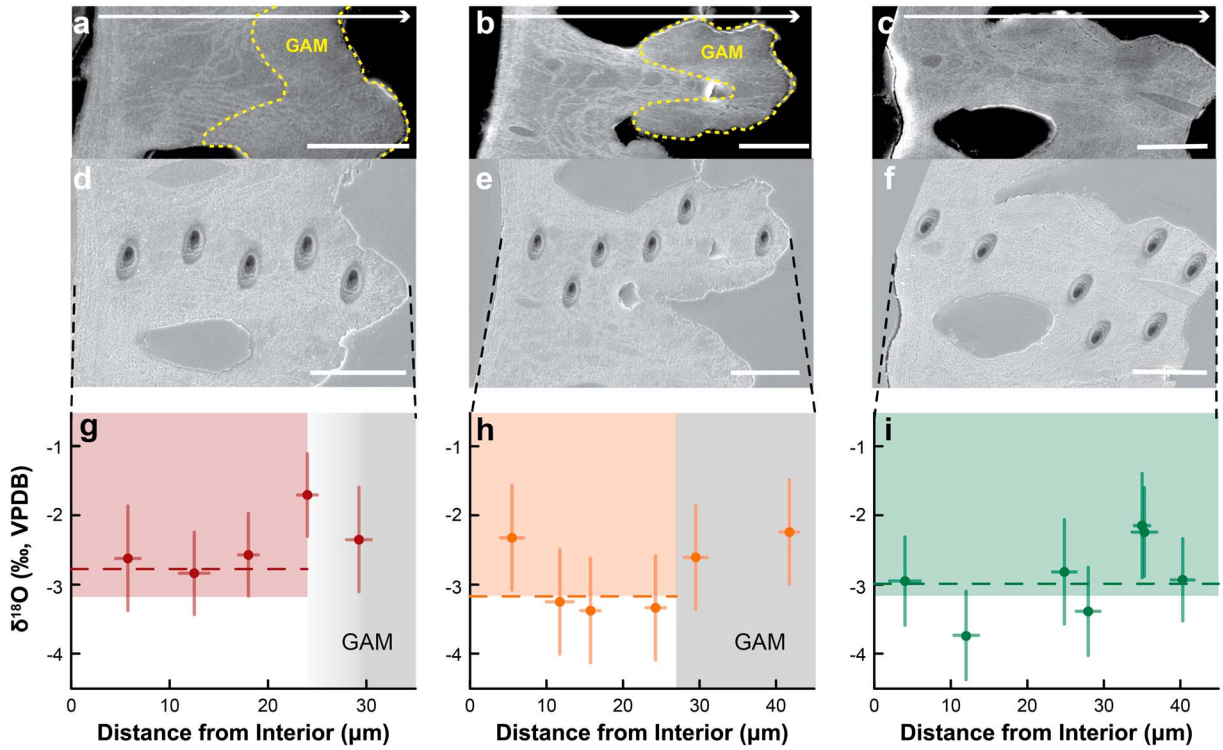

Figure 6. Secondary electron images (a–c) showing cross-sectioned walls of penultimate chambers of three *T. sacculifer* shells from the EqPac sediment trap. Note: GAM crust outlined with yellow dashed line for shells in (a) and (b); shell in (c) is pregametogenic with intact spines (i.e., no GAM crust). Arrows point toward exterior of shells. (d–f) Secondary electron images showing series of 3-μm SIMS pits transecting chamber wall. All scale bars are 10 μm. (g–i) SIMS $\delta^{18}O$ values of pits shown in d–f. Note: All SIMS $\delta^{18}O$ values are adjusted (+0.9‰) using correction determined by Wycech et al. (2018). Average pregametogenic $\delta^{18}O$ value per shell (horizontal dashed line) with predicted range of $\delta^{18}O_{calcite}$ values for 0- to 100-m water depths (color-shaded areas, see section 3.1). Error bars are SIMS external precision (2 SD, vertical) and measured pit width (horizontal). External GAM crust (gray-shaded area) of post-GAM specimens. GAM = gametogenic; SIMS = secondary ion mass spectrometry; VPDB = Vienna Peedee Belemnite.

Step 7: Calculate proportion of PREGAM calcite dissolved by dividing the mapped area of dissolved PREGAM calcite (Step 4) by the total area of penultimate chamber wall (Step 2).

Step 8: Calculate proportion of GAM crust in whole shells before dissolution by dividing the mapped area of GAM calcite (Step 6) by the total area of penultimate chamber wall (Step 2).

With this information, we calculated the percentages of dissolved PREGAM calcite, GAM calcite in whole shells before dissolution, and GAM calcite in whole shells after dissolution for each cross-sectioned *T. sacculifer* (Table S2). Image processing was not performed on nongametogenic shells possessing intact spines (Data Set S1).

3. Results

3.1. Assessing SIMS $\delta^{18}O$ Values Using Sediment Trap *T. sacculifer* Shells

Previous experimentation has shown that 3- and 10-μm SIMS measurements of Holocene-aged shells of the planktic foraminifer *Orbulina universa* yield $\delta^{18}O$ values that, on average, were 0.9 ± 0.1‰ (±2 SE) lower than corresponding GSMS values (Wycech et al., 2018). The cause of this interinstrumental difference is currently a subject of ongoing study, so the possibility of a similar offset should be investigated on a case-by-case basis (Orland et al., 2015). Accordingly, SIMS $\delta^{18}O$ measurements were completed with 3-μm SIMS pits across the penultimate chamber walls of three *T. sacculifer* shells from the EqPac sediment trap (Figure 6). The measured SIMS $\delta^{18}O$ values from PREGAM calcite are compared to the predicted $\delta^{18}O_{calcite}$ values (average = −1.6‰; range = −3.2 to +0.1‰, VPDB) with the latter being calculated using the $\delta^{18}O$ temperature calibration of Mulitza et al. (2003), the annual maximum and minimum temperatures for the upper 100 m of the water

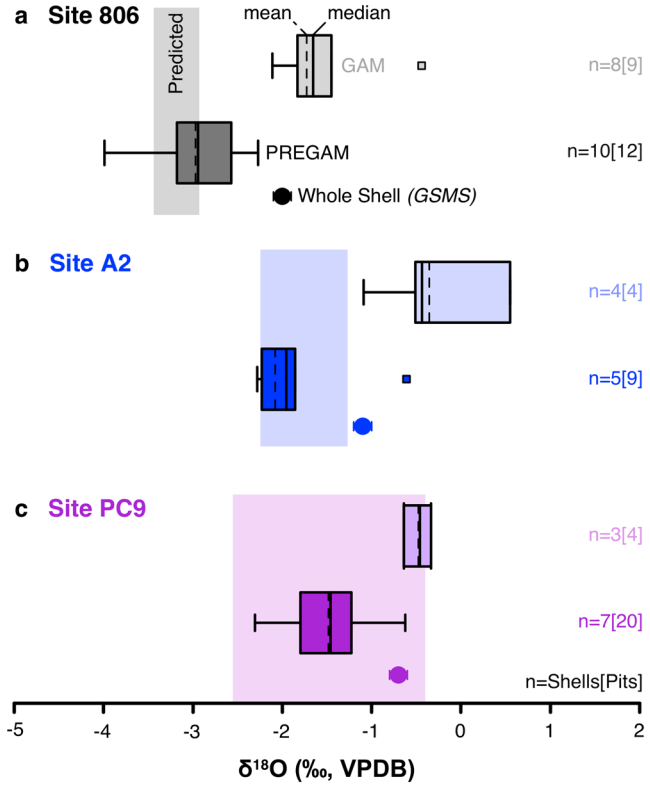

Figure 7. Box and whisker plots of SIMS-based $\delta^{18}O$ values for *T. sacculifer* shells from core top samples at (a) Site 806 (gray), (b) Site A2 (blue), and (c) PC9 (purple). Measured $\delta^{18}O$ values from PREGAM calcite (dark box plots) and GAM calcite (light box plots); median and mean $\delta^{18}O$ values for each sample denoted by solid vertical lines within boxes and dashed vertical lines, respectively. Numerous measurements (pits) were obtained from multiple shells (*n*). Whiskers on boxes are 1.5 times the interquartile range. Outliers are small squares outside of whiskers and are excluded from mean calculation. Comparative whole-shell $\delta^{18}O$ values measured by gas source mass spectrometry (filled circles, see Table 1). Range of predicted $\delta^{18}O$ values (shaded rectangles) calculated using Mulitza et al. (2003) temperature calibration, observed $\delta^{18}O_{sw}$, and observed mean temperatures for 0- to 100-m water depth (annual temperatures at Sites 806 and A2; summer temperatures at Site PC9). GAM = gametogenic; PREGAM = pregametogenic; VPDB = Vienna Peedee Belemnite.

column at the site (22–29 °C; National Oceanic and Atmospheric Administration/Tropical Atmosphere Ocean), and the observed surface ocean $\delta^{18}O_{sw}$ at a nearby site (0.4‰ Vienna standard mean ocean water, Site W8402A-14GC; Dekens et al., 2002). The mean of the uncorrected SIMS $\delta^{18}O$ values measured from the PREGAM calcite of each shell (−3.7‰, −4.1‰, and −3.9‰) are 0.5–0.9‰ lower than the lowest predicted equilibrium $\delta^{18}O_{calcite}$ value (−3.2‰, VPDB). However, applying a 0.9‰ correction to the SIMS data, as in Wycech et al. (2018), brings these PREGAM values into agreement with the predicted $\delta^{18}O_{calcite}$ range, with the average corrected SIMS $\delta^{18}O$ value for each shell (−2.8‰, −3.2‰, and −3.0‰) best approximating the low-$\delta^{18}O_{calcite}$ value calculated from the observed sea surface temperature (SST; Figure 6g to 6i). Thus, corrected SIMS $\delta^{18}O$ values of PREGAM calcite more accurately record upper mixed layer temperatures—the water depth targeted for reconstructions using *T. sacculifer*.

SIMS measurement of both foraminifer calcite and organic/water contaminant phases may partly contribute to the previously reported SIMS-GSMS $\delta^{18}O$ difference (e.g., Orland et al., 2015; Wycech et al., 2018). The $^{16}OH^{-}/^{16}O^{-}$ (OH/O herein) ratios measured by SIMS track the content of hydrogen, which presumably comes from chemically bound water or organic matter within the foraminifer shell, and serve as a secondary method for assessing the validity of a SIMS $\delta^{18}O$ correction to *T. sacculifer* measurements. The OH/O ratios of the EqPac *T. sacculifer* shells are within two standard deviations of the OH/O ratios of the *O. universa* shells analyzed by Wycech et al. (2018; Figure S2, see section S2), suggesting that the organic matter or water content of the calcite composing *T. sacculifer* shells is comparable to that of the calcite composing Holocene age *O. universa* shells. Thus, the SIMS $\delta^{18}O$ correction determined from *O. universa* measurements is deemed appropriate for the SIMS measurements obtained from *T. sacculifer* shells in this study. In short, a correction of +0.9‰ is hereafter applied to all SIMS $\delta^{18}O$ values reported for core top specimens of *T. sacculifer* in this study.

3.2. Comparison of SIMS and Conventional $\delta^{18}O$ Values of Core Top *T. sacculifer*

The average SIMS $\delta^{18}O$ values for the GAM calcite of *T. sacculifer* shells from sites 806, A2, and PC9 are 1.0‰ to 1.4‰ higher than the average SIMS $\delta^{18}O$ values of PREGAM calcite (Figure 7). The intershell variability between the mean PREGAM $\delta^{18}O$ values is 1.8‰ at each study site. Although the GAM $\delta^{18}O$ data set is small (n = 3–8 shells per site), intershell variation in these mean $\delta^{18}O$ values at sites 806 and A2 (1.6–1.7‰) is greater than at Site PC9 (0.3‰). The complementary whole-shell $\delta^{18}O$ values (GSMS) at all three sites fall between the mean PREGAM and GAM $\delta^{18}O$ values, confirming that the whole shells are aggregate mixtures of varying proportions of these two carbonate phases. The intermediate $\delta^{18}O$ values returned by GSMS analyses suggest that these whole shells are composed of more than 50% GAM calcite, but this cursory estimate of the proportion of GAM calcite is considered a rough approximation owing to the possibility that postdepositional diagenetic processes may have skewed some of the whole shell compositions toward higher $\delta^{18}O$ values (see section 4.3).

The measured in situ and whole-shell $\delta^{18}O$ values are compared to the predicted $\delta^{18}O$ calcite values that were calculated using Mulitza et al. (2003), observed $\delta^{18}O_{sw}$ values (Table 1), and observed mean temperatures for 0- to 100-m water depth (annual temperature at sites 806, A2; summer temperature at Site PC9; see Table 1). The mean PREGAM $\delta^{18}O$ measurements fall within the predicted $\delta^{18}O$ range at all sites (Figure 7), whereas the GAM and whole-shell $\delta^{18}O$ values are respectively 1.4‰ and 0.9‰

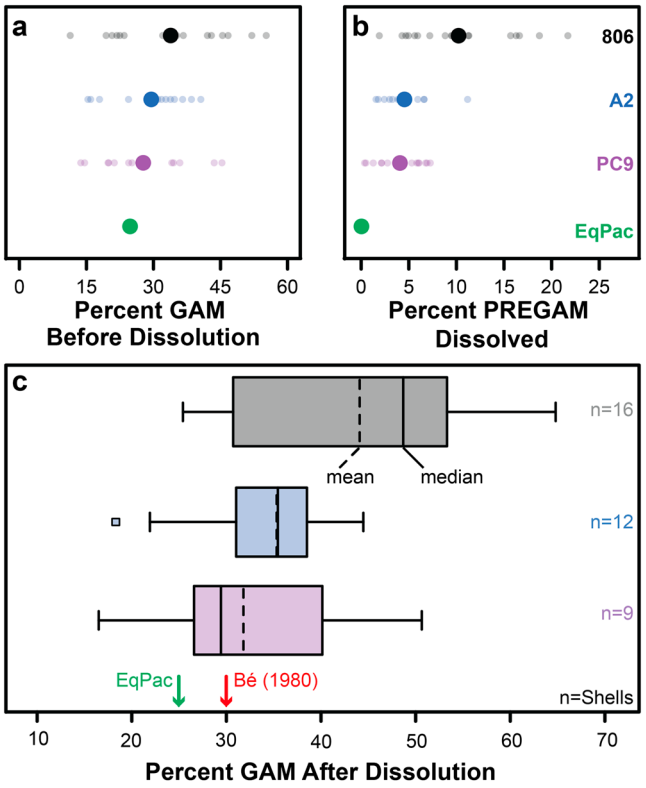

Figure 8. Estimates of GAM percentages and degree of PREGAM dissolution from image processing of penultimate chambers of postgametogenic *T. sacculifer* shells from sites 806 (gray), A2 (blue), PC9 (purple), and EqPac sediment trap (green, $n = 2$ shells). (a) Percentage of GAM before dissolution (small circles = individual shells, large circles = sample averages). (b) Percent PREGAM dissolved (small circles = individual shells, large circles = sample average). (c) Box and whisker plots expressing percentage of GAM in whole shells after dissolution at Sites 806, A2, and PC9. Calculated by addition of paired results in (a) and (b). Arrows show percent GAM estimates from Bé (1980) and EqPac sediment trap. Median and mean values denoted by solid and dashed lines within boxes, respectively. Outliers are small squares outside of whiskers and are excluded from mean calculation. Whiskers on boxes are 1.5 times the interquartile range. GAM = gametogenic; PREGAM = pregametogenic.

higher than the maximum predicted $\delta^{18}O$ value at Site 806 (Figure 7a). Similarly, the GAM and whole-shell $\delta^{18}O$ values are respectively 0.9‰ and 0.2‰ higher than the maximum predicted $\delta^{18}O$ value at Site A2 (Figure 7b). By contrast, the GAM and whole-shell $\delta^{18}O$ values fall at the higher end of the predicted range at Site PC9 (Figure 7c).

3.3. Intersite Differences in Intrashell Dissolution

SEM imaging of the cross sections reveals that the internal layering of many shells has been partially dissolved and that this form of dissolution has preferentially removed PREGAM calcite without altering the external appearance of the shells (Figure 4). Two implications of this form of internal dissolution are as follows: (1) it increases the proportion of GAM calcite composing each shell by removing PREGAM calcite, which further biases whole-shell $\delta^{18}O$ values toward that of the GAM calcite, and (2) it varies between study sites and among shells with differing depositional histories. For instance, SEM imaging of cross-sectioned *T. sacculifer* shells recovered from the EqPac sediment trap shows that these shells have pristine internal structures (Figures 4a and 4b), which is expected since these shells have not experienced postdepositional dissolution on the sea floor. By contrast, the PREGAM calcite layers within the core top shells from sites PC9 and A2 have been partially etched (Figures 4c and 4d). At the other end of the spectrum, core top shells from Site 806 have large voids in regions where there should be solid PREGAM calcite (Figures 4e and 4f).

Image processing of penultimate chambers in the cross-sectioned shells indicates that, on average (±2 SE), GAM calcite composes 25% of the two postgametogenic shells from the EqPac sediment trap, 28 ± 5% of the shells from PC9, 30 ± 5% of the shells from Site A2, and 34 ± 6% of the shells from Site 806 (Figure 8a). However, these initial estimates do not account for the partial dissolution of PREGAM calcite seen in many of the core top shells. While there is no discernable loss of PREGAM calcite from the EqPac shells (Figure 8b), dissolution has removed an average (±2 SE) of 4 ± 1%, 5 ± 1%, and 10 ± 3% of the PREGAM calcite from the penultimate chambers of *T. sacculifer* shells from sites PC9, A2, and 806, respectively (Figure 8b). Given our assumption that only two calcite phases compose *T. sacculifer*, dissolution decreases the percent of PREGAM and equally increases the percent of GAM composing each whole shell. As a result, we revise our initial estimates of the %GAM calcite in core top *T. sacculifer* shells by adding the estimated percentages of PREGAM calcite removed by dissolution to the predissolution estimates of %GAM calcite. After dissolution, the core top *T. sacculifer* shells are composed of ~35% GAM calcite, but percentages vary by site (Figure 8c). On average (±2 SE), shells from Atlantic site PC9 and Caribbean site A2 are respectively composed of 32 ± 5% and 34 ± 4% GAM calcite, whereas *T. sacculifer* shells from Pacific Ocean Site 806 are composed of 44 ± 6% GAM calcite. In summary, the proportion of GAM calcite in whole shells is most similar to the previously published 30% estimate (Bé, 1980) when there is minimal dissolution as in shells from sites A2 and PC9 (Figure 8c), while GAM calcite composes a larger proportion of the shell when dissolution is significant and variable as in shells from Site 806 (Figure 8c).

4. Discussion

4.1. Effect of GAM Calcite on Measured Whole-Shell $\delta^{18}O$ Values

High-$\delta^{18}O$ GAM calcite composes a significant proportion of the whole shell (Figures 8b and 8c) and elevates whole-shell $\delta^{18}O$ values (Figure 7). To quantify the effects of this bias, we calculated whole-shell

Table 2
Summary of In Situ $\delta^{18}O$ Values and Postdissolution Percent GAM Estimates Used to Calculate Whole-Shell $\delta^{18}O$ Values for T. sacculifer Shells From Sites 806, A2, and PC9

Site	Average PREGAM $\delta^{18}O$ (‰, VPDB)	Average GAM $\delta^{18}O$ (‰, VPDB)	Percent GAM after dissolution	n[a]	Calculated whole-shell $\delta^{18}O$ (‰, VPDB)	Measured whole-shell $\delta^{18}O$ (‰, VPDB)	Predicted $\delta^{18}O_{calcite}$ (‰, VPDB)[b]
806	−3.0	−1.7	44.1	5	−2.4	−2.0	−3.4
A2	−2.1	−0.4	35.3	1	−1.5	−1.1	−2.2
PC9	−1.5	−0.5	31.8	3	−1.2	−0.7	−2.6

Note. Measured and predicted $\delta^{18}O$ values provided for comparison. GAM = gametogenic; PREGAM = pregametogenic; VPDB = Vienna Peedee Belemnite.
[a]Number of shells with paired PREGAM-GAM $\delta^{18}O$ values. [b]Calculated with the Mulitza et al. (2003) calibration, sea surface $\delta^{18}O_{sw}$ values and temperatures (mean annual at Sites 806 and A2; mean summer at Site PC9) and reflect the lowest value of the predicted range (Table 1).

$\delta^{18}O$ values by mass balance using measured PREGAM and GAM $\delta^{18}O$ values and the %GAM calcite composing the whole shells after dissolution (Table 2). The calculated whole-shell $\delta^{18}O$ values are within 0.4‰ of the whole-shell $\delta^{18}O$ values measured by GSMS at sites 806 and PC9 and within 0.2‰ of the whole-shell $\delta^{18}O$ values measured by GSMS at Site A2. The reasonably good agreement between the calculated and measured whole-shell $\delta^{18}O$ values speaks to the fidelity of the measured in situ $\delta^{18}O$ values and image processing results. Still, both the calculated and measured whole-shell $\delta^{18}O$ values either exceed or fall at the higher end of predicted $\delta^{18}O$ values at each study site. *T. sacculifer* is typically selected for sea surface reconstructions, but we note that the calculated and measured whole-shell $\delta^{18}O$ values overestimate the minimum $\delta^{18}O$ values predicted for calcite precipitated near the sea surface by 1.0‰ and 1.4‰ at Site 806, 0.9‰ and 1.1‰ at Site A2, and 1.5‰ and 1.9‰ at Site PC9 (see Table 2). Such elevated $\delta^{18}O$ values equate to a 4–8 °C underestimation of observed SSTs. In summation, the presence of GAM crust on *T. sacculifer* shells increases whole-shell $\delta^{18}O$ values, which will ultimately lead to spurious paleoceanographic reconstructions that underestimate SSTs and/or overestimate seawater $\delta^{18}O$ (salinity) values.

4.2. Intersite Differences in Intrashell Dissolution of PREGAM Calcite

The differences between the in situ PREGAM and whole-shell $\delta^{18}O$ data are primarily caused by the presence and variable proportions of high-$\delta^{18}O$ GAM calcite in the shells. Field and culturing studies have provided estimates for the proportion of GAM calcite (28–53%) in whole *T. sacculifer* shells (Bé, 1980; Caron et al., 1990), but these studies did not consider the possibility that the proportion of high-$\delta^{18}O$ GAM calcite in *T. sacculifer* shells may be secondarily increased by the partial dissolution of low-$\delta^{18}O$ PREGAM calcite (Johnstone et al., 2010, 2011; Lorens et al., 1977). This potential bias is confirmed by SEM imaging of *T. sacculifer* shells in cross section, which shows that the degree of PREGAM dissolution varies between sites and is most severe in shells from Site 806 (Figure 4). Thus, the results presented in this study clearly demonstrate that postdepositional dissolution acts to elevate the proportion of GAM calcite composing whole *T. sacculifer* shells by selectively removing PREGAM calcite (Figure 8).

Why PREGAM calcite is more susceptible to dissolution than GAM calcite remains unclear, but the selectivity of this dissolution is likely related to the oxidation of organic matter within internal domains and/or the microcrystalline structure and higher Mg composition of PREGAM calcite (Branson et al., 2016; Johnstone et al., 2010, 2011; Nouet & Bassinot, 2007). Moreover, previous study has shown that diurnal variation in the biological activity of algal symbionts hosted by many mixed layer dwelling planktic foraminifers imparts sequential day-night banding to the PREGAM calcite, with the night bands having higher Mg content (Eggins et al., 2004; Spero et al., 2015; Fehrenbacher et al., 2017). The partial dissolution (etching) observed along discrete layers within the PREGAM portion of some *T. sacculifer* shells is consistent with the argument for preferential dissolution of more soluble, banded domains (Figures 4c–4f and Data Set S2).

The possibility that night bands are preferentially dissolved warrants consideration because calcite formed at night typically composes about one third of the PREGAM portion of the shell and is ~1‰ higher in $\delta^{18}O$ than the calcite formed during the day due to diurnal symbiont activity (Spero & Lea, 1993). Complete dissolution of only the more soluble, night calcite would decrease the PREGAM $\delta^{18}O$ value by 0.3‰ because the process is removing a third of the calcite that is 1‰ higher than the remaining PREGAM calcite. However, the dissolution of the PREGAM calcite increases the proportion of high-$\delta^{18}O$ GAM calcite in the whole shell. For

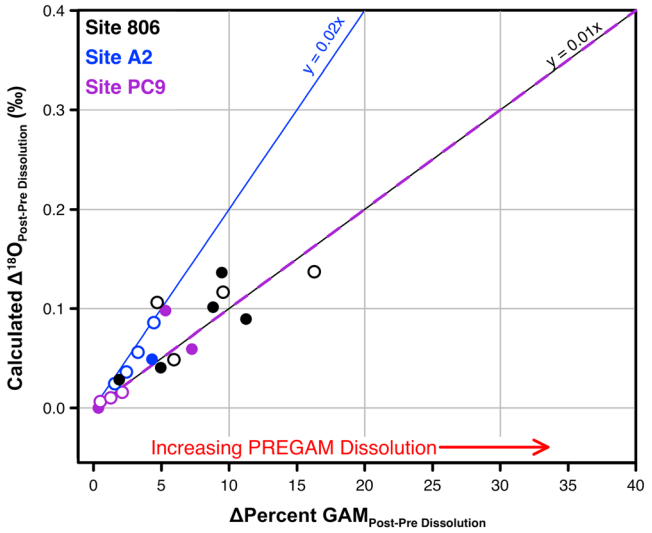

Figure 9. Scatterplot of the difference in whole-shell $\delta^{18}O$ before and after dissolution ($\Delta^{18}O_{post\text{-}pre\ dissolution}$) as a function of the change in percent GAM (ΔPercent $GAM_{post\text{-}pre\ dissolution}$) for *T. sacculifer* shells from Sites 806 (black), A2 (blue), and PC9 (purple). $\Delta^{18}O$ values calculated by mass balance with in situ PREGAM and GAM $\delta^{18}O$ values (Table S1) and percent GAM values before and after dissolution (Figures 8a and 8c; Table S2). Paired PREGAM-GAM $\delta^{18}O$ values from the same shell (filled circles). In cases when in situ measurements were not paired within a shell, the mean $\delta^{18}O$ value of the unmeasured calcite phase for the site was used to calculate $\Delta^{18}O$ (open circles). Mean slopes for sites 806/PC9 (black/purple line) and Site A2 (blue line). GAM = gametogenic; PREGAM = pregametogenic.

example, if a pristine whole shell is composed of 70% PREGAM and 30% GAM, the same whole shell is composed of 47% PREGAM (two thirds of 70%) and 53% GAM (100% minus remaining %PREGAM) after the dissolution of only the night calcite. The change to the whole-shell $\delta^{18}O$ value is calculated as

$$\Delta^{18}O_{WS} = \delta^{18}O_{WS\ PostDiss} - \delta^{18}O_{WS\ PreDiss},$$

where $\Delta^{18}O_{WS}$ is the change in whole-shell $\delta^{18}O$ value due to dissolution, $\delta^{18}O_{WS\ PostDiss}$ is the whole-shell $\delta^{18}O$ value after dissolution, and $\delta^{18}O_{WS\ PreDiss}$ is the whole-shell $\delta^{18}O$ value before dissolution. Mass balance equations are substituted for $\delta^{18}O_{WS\ PostDiss}$ and $\delta^{18}O_{WS\ PreDiss}$,

$$\Delta^{18}O_{WS} = \left[\frac{2}{3}f_{PG}\delta^{18}O_{PG} + \left(1 - \frac{2}{3}f_{PG}\right)\delta^{18}O_G\right] - \left[f_{PG}\delta^{18}O_{PG} + (1 - f_{PG})\delta^{18}O_G\right],$$

where f_{PG} is the proportion of PREGAM calcite composing the whole shells before dissolution and $\delta^{18}O_{PG}$ and $\delta^{18}O_G$ are the $\delta^{18}O$ values of the PREGAM and GAM calcites before dissolution, respectively. The equation simplifies to

$$\Delta^{18}O_{WS} = \frac{1}{3}f_{PG}\delta^{18}O_G - \frac{1}{3}f_{PG}\delta^{18}O_{PG}.$$

Given the difference of PREGAM and GAM $\delta^{18}O$ values (1–1.4‰) and pre-dissolution %PREGAM calcite (66–72%) of the *T. sacculifer* shells recovered from the core top samples in this study, dissolution of only the night bands within the PREGAM calcite would increase the whole-shell GSMS $\delta^{18}O$ value by 0.2–0.3‰. This estimate is supported by Figure 9 in which in situ $\delta^{18}O$ values and results of image processing (Figures 8b and 8c) are used to calculate whole-shell $\delta^{18}O$ values before and after dissolution. Results indicate that a 10% increase in GAM calcite due to dissolution increases whole-shell $\delta^{18}O$ values by 0.1‰ at sites 806 and PC9, and 0.2‰ at Site A2 (Figure 9). These estimates suggest that the preferential dissolution of high-$\delta^{18}O$ night bands affects whole-shell $\delta^{18}O$ values by only 0.1–0.2‰ when ~10% of PREGAM calcite is removed. While the evidence at hand suggests that PREGAM dissolution has a relatively minor effect on whole-shell $\delta^{18}O$ compositions, it is highly plausible that *T. sacculifer* shells recovered from a dissolution-prone site may have been *hollowed out* by the removal of PREGAM calcite. Under such extreme conditions, the wholesale dissolution of PREGAM calcite will have an even greater impact on whole-shell $\delta^{18}O$ values (Figure 9).

4.3. Caveats and Implications

Another diagenetic process that affects whole foraminiferal $\delta^{18}O$ values is the postdepositional addition of secondary, inorganic calcite. With the notable exception of shells from the EqPac sediment trap sample and 50% of the shells from Site PC9, the shells analyzed from the core top samples are opaque (white) under optical light—indicative of early diagenetic alteration (in the sense of Pearson et al., 2001, 2007; Sexton et al., 2006; Wycech et al., 2016). Thus, the whole-shell $\delta^{18}O$ values may be slightly elevated due to partial contamination from the addition of high $\delta^{18}O$-diagenetic calcite, which may explain why the image processing estimates of %GAM calcite in whole shells are lower (32–44% GAM, Figure 8c) than those suggested by comparison of GSMS and in situ $\delta^{18}O$ values (≥50% GAM, Figure 7).

Nevertheless, the results of this study provide tighter constraints on the findings of earlier studies (e.g., Duplessy et al., 1981; Lohmann, 1995), which have argued that the proportion of GAM calcite is an important source of intersample and intersite variability seen in whole-shell *T. sacculifer* $\delta^{18}O$ records. Predictably, GAM calcite will also have a deleterious effect on whole-shell $\delta^{18}O$ values of other foraminiferal species that undergo large depth migrations. In light of our results, direct comparison of whole-shell $\delta^{18}O$ values from

different ocean basins (i.e., Site 806 versus Sites A2 and PC9) requires investigation into and correction for PREGAM dissolution. Relative to the Atlantic Ocean and Caribbean, the older and more corrosive deep waters of the Pacific Ocean result in shells that have less PREGAM calcite (Figure 8b), more GAM calcite (Figure 8c), and whole-shell $\delta^{18}O$ values that are more strongly biased toward the high-$\delta^{18}O$ GAM calcite phase (Figure 7). Spatiotemporal trends in whole-shell $\delta^{18}O$ values of *T. sacculifer* are often related to changes in the ocean climate system (e.g., Groeneveld et al., 2008; Keigwin, 1982; Wara et al., 2005), but such inferences should not be made without verification of comparable internal shell preservation between samples and sites. This is especially true for geochemical studies entailing whole shell analyses of planktic foraminifer species that grow a dissolution-resistant crust over the exterior of their shells. We recommend that future studies mount and cross section a subsample of the shells to be analyzed and assess their preservation by SEM imaging. The images and results presented in this study provide the means to correct whole-shell $\delta^{18}O$ values for dissolution and the addition of GAM calcite in *T. sacculifer*.

5. Conclusions

This study reports the first in situ $\delta^{18}O$ measurements of two biogenic calcite phases (PREGAM and GAM) composing individual shells of the planktic foraminifer species, *T. sacculifer*. These in situ $\delta^{18}O$ measurements were performed on micrometer-sized (~3–10 μm) domains of individual shells using SIMS. We assess the validity of a previously determined SIMS $\delta^{18}O_{calcite}$ correction (+0.9‰; Wycech et al., 2018) by measuring the PREGAM calcite of sediment trap *T. sacculifer* shells. We find that corrected SIMS $\delta^{18}O$ values more accurately record upper mixed layer temperatures—the water depth targeted for reconstructions using *T. sacculifer*. Thus, all SIMS $\delta^{18}O$ values herein reported have been adjusted accordingly.

SIMS analyses performed on *T. sacculifer* shells recovered from Holocene-aged sediments of three study sites show that the $\delta^{18}O$ of GAM calcite added to shells during the terminal stage of the life cycle is 1.0–1.4‰ higher than that of PREGAM calcite. The large intrashell $\delta^{18}O$ variability is primarily due to precipitation of the GAM crust in deeper (cooler) water. Complementary whole-shell measurements yield intermediate $\delta^{18}O$ values that fall between in situ $\delta^{18}O$ values measured from PREGAM and GAM calcites at all three study sites. This result confirms that *T. sacculifer* shells are aggregate mixtures of PREGAM and GAM calcites and that whole-shell $\delta^{18}O$ values are elevated by the addition of high-$\delta^{18}O$ GAM calcite.

Examination of shells in cross section reveals that most have suffered varying degrees of PREGAM calcite dissolution. This form of preferential dissolution may go undetected when using traditional microscopy because it dissolves shells from the inside-out without altering external surface textures. This is especially true for planktic foraminifer species, such as *T. sacculifer*, that have a dissolution-resistant crust of GAM calcite covering the exterior of their shells. Such dissolution potentially increases the PREGAM-GAM $\delta^{18}O$ difference within shells, secondarily increases the proportion of high-$\delta^{18}O$ GAM calcite composing whole shells, and elevates whole-shell $\delta^{18}O$ values. Furthermore, the degree of PREGAM dissolution varies between study sites and is most severe at the Pacific Ocean site.

Results of this study highlight long-standing issues with paleoclimate reconstructions derived from conventional whole-shell $\delta^{18}O$ measurements of postgametogenic *T. sacculifer*. By the same token, this case study demonstrates how in situ $\delta^{18}O$ measurement of PREGAM calcite provides a novel technique to enhance the fidelity of records of past surface ocean conditions and, when combined with quantitative image processing, a means to account for the $\delta^{18}O$ value and proportion of GAM calcite composing whole *T. sacculifer* shells.

Acknowledgments
Funding was courtesy of the Geological Society of America Graduate Student Grant (Wycech), the University of Wisconsin-Madison Geoscience Department Graduate Student Summer Research Fund (Wycech), and Shell Oil Company (Kelly). WiscSIMS is supported by the National Science Foundation (EAR-1355590 and EAR-1658823) and the University of Wisconsin—Madison. Brian Hess prepared epoxy mounts. Noriko Kita assisted with SIMS measurements. Shipboard coring operations for PC9 was supported by the United States Geological Survey (William Dillon) and Woods Hole Oceanographic Institute (Richard Norris, Kelly). The crew of the RV *Cape Hatteras*, Charles Paull, and William Ussler conducted PC9 coring operations. The piston core at Site A2 was collected by Woods Hole Oceanographic Institute (S. Downey). Some of the samples used in this study were provided by the International Ocean Discovery Program (IODP). We also thank Ellen Roosen (WHOI Core Repository) for core sampling assistance. EqPac sediment trap sample was courtesy of Steven Manganini (WHOI). Site 806 and EqPac observed temperatures from Tropical Atmosphere Ocean Array (GTMBA Project Office of NOAA/PMEL). Conventional stable isotope measurements for sites A2 and PC9 was performed by Dyke Andreason (University of California, Santa Cruz). We also thank Brett Metcalfe and one anonymous reviewer for their suggestions that helped improve the manuscript. SEM images and data tables are included as supporting information. The $\delta^{18}O$ data are also available in the National Center for Environmental Information Database (ncdc.noaa.gov/paleo/study/25410).

References

Anand, P., Elderfield, H., & Conte, M. H. (2003). Calibration of Mg/Ca thermometry in planktonic foraminifera from a sediment trap time series. *Paleoceanography*, *18*(2), 1050. https://doi.org/10.1029/2002PA000846

Bé, A. W. (1960). Ecology of recent planktonic foraminifera: Part 2: Bathymetric and seasonal distributions in the Sargasso Sea off Bermuda. *Micropaleontology*, *6*(4), 373–392. https://doi.org/10.2307/1484218

Bé, A. W. (1980). Gametogenic calcification in a spinose planktonic foraminifer, *Globigerinoides sacculifer* (Brady). *Marine Micropaleontology*, *5*, 283–310. https://doi.org/10.1016/0377-8398(80)90014-6

Bé, A. W., Spero, H., & Anderson, O. (1982). Effects of symbiont elimination and reinfection on the life processes of the planktonic foraminifer *Globigerinoides sacculifer*. *Marine Biology*, *70*(1), 73–86. https://doi.org/10.1007/BF00397298

Berger, W. H. (1968). Planktonic foraminifera: Selective solution and paleoclimatic interpretation. *Deep-Sea Research*, *15*(1), 31–43. https://doi.org/10.1016/0011-7471(68)90027-2

Berger, W. H. (1970). Planktonic foraminifera: Differential production and expatriation off Baja California. *Limnology and Oceanography*, *15*(2), 183–204. https://doi.org/10.4319/lo.1970.15.2.0183

Berger, W. H., Bonneau, M. C., & Parker, F. L. (1982). Foraminifera on the deep-sea floor: Lysocline and dissolution rate. *Oceanologica Acta*, *5*, 249–258.

Bijma, J., & Hemleben, C. (1994). Population dynamics of the planktic foraminifer *Globigerinoides sacculifer* (Brady) from the Central Red Sea. *Deep-Sea Research*, *41*(3), 485–510. https://doi.org/10.1016/0967-0637(94)90092-2

Branson, O., Bonnin, E. A., Perea, D. E., Spero, H. J., Zhu, Z., Winters, M., Hönisch, B. R., et al. (2016). Nanometer-scale chemistry of a calcite biomineralization template: Implications for skeletal composition and nucleation. *Proceedings of the National Academy of Sciences*, *13*(06), 428–436. https://doi.org/10.1017/S1431927607070845.

Caron, D. A., Anderson, O. R., Lindsey, J. L., Faber, W. W. Jr., & Lim, E. L. (1990). Effects of gametogenesis on test structure and dissolution of some spinose planktonic foraminifera and implications for test preservation. *Marine Micropaleontology*, *16*(1-2), 93–116. https://doi.org/10.1016/0377-8398(90)90031-G

Dekens, P. S., Lea, D. W., Pak, D. K., & Spero, H. J. (2002). Core top calibration of Mg/Ca in tropical foraminifera: Refining paleotemperature estimation. *Geochemistry, Geophysics, Geosystems*, *3*(4), 1022. https://doi.org/10.1029/2001GC000200

Deuser, W. G., & Ross, E. H. (1989). Seasonally abundant planktonic foraminifera of the Sargasso Sea: Succession, deep-water fluxes, isotopic compositions, and paleoceanographic implications. *Journal of Foraminiferal Research*, *19*(4), 268–293. https://doi.org/10.2113/gsjfr.19.4.268

Duplessy, J. C., Blanc, P.-L., & Bé, A. W. (1981). Oxygen-18 enrichment of planktonic foraminifera due to gametogenic calcification below the euphotic zone. *Science*, *213*(4513), 1247–1250. https://doi.org/10.1126/science.213.4513.1247

Eggins, S., Sadekov, A., & De Deckker, P. (2004). Modulation and daily banding of Mg/Ca in tests by symbiont photosynthesis and respiration: A complication for seawater thermometry? *Earth and Planetary Science Letters*, *225*(3–4), 411–419. https://doi.org/10.1016/j.epsl.2004.06.019

Elderfield, H., Vautravers, M., & Cooper, M. (2002). The relationship between shell size and Mg/Ca, Sr/Ca, $\delta^{18}O$, and $\delta^{13}C$ of species of planktonic foraminifera. *Geochemistry, Geophysics, Geosystems*, *3*(8), 1052. https://doi.org/10.1029/2001GC000194

Fehrenbacher, J. S., Russell, A. D., Davis, C. V., Gagnon, A. C., Spero, H. J., Cliff, J. B., Zhu, Z., et al. (2017). Link between light-triggered Mg-banding and chamber formation in the planktic foraminifera *Neogloboquadrina dutertrei*. *Nature Communications*, *8*(15441), 1–10. https://doi.org/10.1038/ncomms15441

Ford, H. L., Ravelo, A. C., & Polissar, P. J. (2015). Reduced El Niño–Southern Oscillation during the Last Glacial Maximum. *Science*, *347*(6219), 255–258. https://doi.org/10.1126/science.1258437

Groeneveld, J., Nurnberg, D., Tiedemann, R., Reichart, G. J., Steph, S., Reuning, L., et al. (2008). Foraminiferal Mg/Ca increase in the Caribbean during the Pliocene: Western Atlantic Warm Pool formation, salinity influence, or diagenetic overprint? *Geochemistry Geophysics Geosystems*, *9*, Q01P23. https://doi.org/10.1029/2006GC001564

Honjo, S., Dymond, J., Collier, R., & Manganini, S. J. (1995). Export production of particles to the interior of the equatorial Pacific Ocean during the 1992 EqPac experiment. *Deep Sea Research, Part II*, *42*(2–3), 831–870. https://doi.org/10.1016/0967-0645(95)00034-N

Johnstone, H. J. H., Schulz, M., Barker, S., & Elderfield, H. (2010). Inside story: An X-ray computed tomography method for assessing dissolution in the tests of planktonic foraminifera. *Marine Micropaleontology*, *77*(1–2), 58–70. https://doi.org/10.1016/j.marmicro.2010.07.004

Johnstone, H. J. H., Yu, J., Elderfield, H., & Schulz, M. (2011). Improving temperature estimates derived from Mg/Ca of planktonic foraminifera using X-ray computed tomography–based dissolution index, XDX. *Paleoceanography*, *26*, PA1215. https://doi.org/10.1029/2009PA001902

Keigwin, L. (1982). Isotopic paleoceanography of the Caribbean and East Pacific: Role of Panama uplift in Late Neogene time. *Science*, *217*(4557), 350–353. https://doi.org/10.1126/science.217.4557.350

Kita, N. T., Ushikubo, T., Fu, B., & Valley, J. W. (2009). High precision SIMS oxygen isotope analysis and the effect of sample topography. *Chemical Geology*, *264*(1–4), 43–57. https://doi.org/10.1016/j.chemgeo.2009.02.012

Kozdon, R., Kelly, D. C., Kita, N. T., Fournelle, J. H., & Valley, J. W. (2011). Planktonic foraminiferal oxygen isotope analysis by ion microprobe technique suggests warm tropical sea surface temperatures during the Early Paleogene. *Paleoceanography*, *26*, PA3206. https://doi.org/10.1029/2010PA002056

Kozdon, R., Kelly, D. C., Kitajima, K., Strickland, A., Fournelle, J. H., & Valley, J. W. (2013). In situ $\delta^{18}O$ and Mg/Ca analyses of diagenetic and planktic foraminiferal calcite preserved in a deep-sea record of the Paleocene-Eocene thermal maximum. *Paleoceanography*, *28*, 517–528. https://doi.org/10.1002/palo.20048

Kozdon, R., Ushikubo, T., Kita, N. T., Spicuzza, M. J., & Valley, J. W. (2009). Intratest oxygen isotope variability in the planktonic foraminifer *N. pachyderma*: Real vs. apparent vital effects by ion microprobe. *Chemical Geology*, *258*(3–4), 327–337. https://doi.org/10.1016/j.chemgeo.2008.10.032

Lea, D. W., Pak, D. K., & Spero, H. J. (2000). Climate impact of Late Quaternary equatorial Pacific sea surface temperature variations. *Science*, *289*(5485), 1719–1724. https://doi.org/10.1126/science.289.5485.1719

Locarnini, R. A., Mishonov, A. V., Antonov, J. I., Boyer, T. P., Garcia, H. E., Baranova, O. K., Zweng, M. M., et al. (2013). *World ocean atlas 2013, volume 1: Temperature*. S. Levitus, Ed., A. Mishonov Technical Ed.; NOAA Atlas NESDIS 73 (40 pp.).

Lohmann, G. P. (1995). A model for variation in the chemistry of planktonic foraminifera due to secondary calcification and selective dissolution. *Paleoceanography*, *10*(3), 445–457. https://doi.org/10.1029/95PA00059

Lorens, R. B., Williams, D. F., & Bender, M. (1977). The early nonstructural chemical diagenesis of foraminiferal calcite. *Journal of Sedimentary Petrology*, *47*(4), 1602–1609. https://doi.org/10.1306/212F73C9-2B24-11D7-8648000102C1865D

Mulitza, S., Boltovskoy, D., Donner, B., Meggers, H., Paul, A., & Wefer, G. (2003). Temperature: $\delta^{18}O$ relationships of planktonic foraminifera collected from surface waters. *Palaeogeography, Palaeoclimatology, Palaeoecology*, *202*(1-2), 143–152. https://doi.org/10.1016/S0031-0182(03)00633-3

Nouet, J., & Bassinot, F. (2007). Dissolution effects on the crystallography and Mg/Ca content of planktonic foraminifera *Globorotalia tumida* (Rotaliina) revealed by X-ray diffractometry. *Geochemistry, Geophysics, Geosystems*, *8*, Q10007. https://doi.org/10.1029/2007GC001647

Orland, I., Kozdon, R., Linzmeier, B. J., Wycech, J., Sliwiński, M. G., Kitajima, K., et al. (2015). Enhancing the accuracy of carbonate $\delta^{18}O$ and $\delta^{13}C$ measurements by SIMS (pp. 1–2). Presented at the American Geophysics Union.

Pearson, P. N., Ditcheld, P. W., Singano, J., Harcourt-Brown, K. G., Nicholas, C. J., Shackleton, N. J., & Hall, M. A. (2001). Warm tropical sea surface temperatures in the Late Cretaceous and Eocene epochs. *Nature*, *415*, 481–487.

Pearson, P. N., Van Dongen, B. E., Nicholas, C. J., Pancost, R. D., Schouten, S., Singano, J. M., & Wade, B. S. (2007). Stable warm tropical climate through the Eocene epoch. *Geology*, *35*(3), 211–214. https://doi.org/10.1130/G23175A.1

Sexton, P. F., Wilson, P. A., & Pearson, P. N. (2006). Microstructural and geochemical perspectives on planktic foraminiferal preservation: "Glassy" versus "Frosty". *Geochemistry, Geophysics, Geosystems*, *7*, Q12P19. https://doi.org/10.1029/2006GC001291

Shipboard Scientific Party (1991). Site 806. In L. W. Kroenke, et al. (Eds.), *Proceedings of the Ocean Drilling Program, Initial Reports* (Vol. 130, pp. 291–367). College Station, TX: Ocean Drilling Program. https://doi.org/10.2973/odp.proc.ir.130.108.1991

Spero, H., & Lea, D. W. (1993). Intraspecific stable isotope variability in the planktic foraminifera *Globigerinoides sacculifer*: Results from laboratory experiments. *Marine Micropaleontology*, *22*(3), 221–234. https://doi.org/10.1016/0377-8398(93)90045-Y

Spero, H. J., Eggins, S. M., Russell, A. D., Vetter, L., Kilburn, M. R., & Honisch, B. (2015). Timing and mechanism for intratest Mg/Ca variability in a living planktic foraminifer. *Earth and Planetary Science Letters*, *409*(C), 32–42. https://doi.org/10.1016/j.epsl.2014.10.030

Spezzaferri, S., Kucera, M., Pearson, P. N., Wade, B. S., Rappo, S., Poole, C. R., et al. (2015). Fossil and genetic evidence for the polyphyletic nature of the planktonic foraminifera "*Globigerinoides*," and description of the new genus *Trilobatus*. *PLoS One*, *10*(5), 1–20. https://doi.org/10.1371/journal.pone.0128108.s004

Thunell, R. C., & Honjo, S. (1981). Calcite dissolution and the modification of planktonic foraminiferal assemblages. *Marine Micropaleontology*, *6*(2), 169–182. https://doi.org/10.1016/0377-8398(81)90004-9

Wara, M. W., Ravelo, A. C., & Delaney, M. G. L. (2005). Permanent El Niño-like conditions during the Pliocene warm period. *Science*, *309*(5735), 758–761. https://doi.org/10.1126/science.1112596

Wycech, J., Kelly, D. C., & Marcott, S. (2016). Effects of seafloor diagenesis on planktic foraminiferal radiocarbon ages. *Geology*, *44*(7), 551–554. https://doi.org/10.1130/G37864.1

Wycech, J. B., Kelly, D. C., Kozdon, R., Orland, I. J., Spero, H. J., & Valley, J. W. (2018). Comparison of $\delta^{18}O$ analyses on individual planktic foraminifer (*Orbulina universa*) shells by SIMS and gas-source mass spectrometry. *Chemical Geology*, *483*, 119–130. https://doi.org/10.1016/j.chemgeo.2018.02.028